

Available online at [www.sciencedirect.com](http://www.sciencedirect.com)
[www.elsevier.com/locate/jmbbm](http://www.elsevier.com/locate/jmbbm)

## Research paper

# Simultaneous microstructural and mechanical characterization of human corneas at increasing pressure

Aurélie Benoit<sup>a,1</sup>, Gaël Latour<sup>b,c,1</sup>, Marie-Claire Schanne-Klein<sup>b</sup>,  
Jean-Marc Allain<sup>a,\*</sup>

<sup>a</sup>LMS, École polytechnique, CNRS, Université Paris-Saclay, 91128 Palaiseau, France

<sup>b</sup>LOB, École polytechnique, CNRS, Inserm U1128, Université Paris-Saclay, 91128 Palaiseau cedex, France

<sup>c</sup>IMNC, Univ. Paris-Sud, Univ. Paris-Diderot, CNRS, Université Paris-Saclay, 91405 Orsay cedex, France

## ARTICLE INFO

### Article history:

Received 20 July 2015

Received in revised form

23 September 2015

Accepted 22 December 2015

Available online 31 December 2015

### Keywords:

Cornea

Biomechanics

Non-linear microscopy

Collagen

Microstructure

Digital image correlation

## ABSTRACT

The cornea, through its shape, is the main contributor to the eye's focusing power. Pathological alterations of the cornea strongly affect the eye power. To improve treatments, complex biomechanical models have been developed based on the architecture and mechanical properties of the collagen network in the stroma, the main layer of the cornea. However, direct investigations of the structure of the stroma, as well as its link to the mechanical response, remained limited. We propose here an original set up, associating nonlinear optical imaging and mechanical testing. By using polarization resolved Second Harmonic signals, we simultaneously quantified micrometer (orientation of the collagen lamellae) and nanometer (local disorder within lamellae) scale corneal organization. We showed that the organization of the lamellae changes along the stroma thickness. Then, we measured simultaneously the deformation on the epithelial side of the cornea and the reorientation of the collagen lamellae for increasing intraocular pressure levels, from physiological ones to pathological ones. We showed that the observed deformation is not correlated to initial orientation, but to the reorganization of the lamellae in the stroma. Our results, by providing a direct multi-scale observation, will be useful for the development of more accurate biomechanical models.

© 2016 Elsevier Ltd. All rights reserved.

## 1. Introduction

The cornea is the anterior part of the eye and is characterized by two main optical properties: transparency and focalization

of light. It contributes to approximately two third of the optical power of the eye. Any modification in the shape or the mechanical strength of cornea induces a loss of vision. It is the case in several pathologies that are related to abnormal

\*Corresponding author.

E-mail address: [allain@lms.polytechnique.fr](mailto:allain@lms.polytechnique.fr) (J.-M. Allain).

<sup>1</sup>Aurélie Benoit and Gaël Latour contributed equally to this work.

intraocular pressure (IOP), as glaucoma, or to variations of the structural and mechanical properties of the cornea, as keratoconus (Daxer and Fratzl, 1997; Meek et al., 2005; Morishige et al., 2014). Another clinical issue is corneal wound healing after laser refractive surgery procedures or corneal graft (Roberts, 2000). The mechanical strength and the shape of the cornea are tightly related to the highly organized three-dimensional architecture of the corneal stroma. This layer represents 90% of the corneal thickness, between the epithelium and the Bowman's membrane on the anterior side, and the Descemet's membrane and the endothelium on the posterior side (Krachmer et al., 2005). It is composed of hundreds of 2–3  $\mu\text{m}$ -thick stacked collagen lamellae containing aligned nanometric collagen fibrils. Any disruption of the stroma microstructure is expected to affect the mechanical and optical properties of the cornea. It is therefore of great interest to develop specific and contrasted imaging tools to probe and quantify these hierarchical collagen structures in relationship with the corneal mechanical behavior.

The corneal microstructure has been first, to the best of our knowledge, investigated using electron microscopy (Beuerman and Pedroza, 1996; Radner et al., 1998). X-ray scattering patterns obtained by using Synchrotron radiation source (Meek and Boote, 2009) have also provided information about the anisotropic arrangements of collagen lamellae through the whole stroma in different regions of the cornea. Nevertheless, both techniques required tissue fixation preventing any mechanical assays. More recently, second harmonic generation (SHG) microscopy, a particular type of nonlinear optical microscopy, has proven to be an efficient tool for obtaining virtual biopsies in unstained fresh corneas (Aptel et al., 2010; Han et al., 2005; Latour et al., 2012b; Matteini et al., 2009; Morishige et al., 2014; Winkler et al., 2013, 2015; Yeh et al., 2002). All these studies have shown the complex and multiscale organization of human cornea, with lamellae mainly oriented along two orthogonal directions near the center, and mostly circumferentially near the sclera at the border (Quantock et al., 2015).

Elaborate biomechanical models (Nguyen and Boyce, 2011; Pandolfi and Vasta, 2012; Petsche and Pinsky, 2013; Pinsky et al., 2005; Studer et al., 2010; Whitford et al., 2015) have been developed recently to deal with both the stromal microstructure and the curved geometry of the cornea. They assumed a given distribution of lamellae and a hyperelastic behavior for the collagen fibrils. Calibration and validation of these models required experimental characterization of cornea mechanical behavior. Using controlled environment and loading conditions, *ex vivo* experiments have investigated various mechanical parameters through inflation (Boyce et al., 2008; Elsheikh et al., 2007, 2010; Hjortdal, 1995, 1996; Hjortdal and Jensen, 1995; Shin et al., 1997) or shear tests (Elsheikh et al., 2009; Petsche et al., 2012). In most inflation studies, the corneal surface strain was deduced from the apex displacement under increasing IOP (Elsheikh et al., 2007, 2010). Boyce et al. (2008) measured surface strains on bovine corneas using digital image correlation, whereas Hjortdal (Hjortdal, 1995, 1996; Hjortdal and Jensen, 1995) and Shin et al. (1997) reported pressure-induced mechanical strain on human corneas, using particle tracking on the epithelial side. More recent studies focused on *in vivo* mechanical

characterization, using clinical devices (Pinero and Alcon, 2014), shear wave imaging (Nguyen et al., 2014) or full-field OCT combined with elastography (Nahas et al., 2013). Nevertheless, to our knowledge, all biomechanical models of cornea combined microstructural and mechanical information measured in distinct corneas. Therefore, significant progresses could be achieved on the validation and calibration of these models by being able to track the evolution of the corneal microstructure, and in particular of the lamellae orientation, during a mechanical loading.

To address this issue and determine in a reliable way the relationship between the collagen organization at nano- and micrometer scale in corneal stroma and the mechanical properties of this tissue, we present here semi-continuous observations of the evolution of the microstructure of the stroma during mechanical inflation tests on fresh human corneas. To that end, we combined SHG microscopy with mechanical assays and monitored simultaneously the stroma microstructure and the mechanical response. By tracking fluorescent micro-beads deposited on corneal epithelium, strains were measured on the anterior surface of the cornea for IOP varying from physiological to highly pathological levels. Quantitative structural information at both nanometer and micrometer scales were obtained by polarization-resolved SHG (P-SHG) microscopy, in particular the orientation of the collagen fibrils that form the collagen lamellae (Gusachenko et al., 2012; Stoller et al., 2002). By mapping this orientation at sequential depths within the cornea, we measured the probability density of fibril orientation along the whole depth of the cornea (Latour et al., 2012b). We then correlated structural and mechanical data obtained at different scales to get insight about the multiscale mechanics of each studied cornea. We showed that the distribution of fibril orientation changed from anterior to posterior stroma, indicating a transition from an isotropic to a more orthotropic microstructure. We also showed that the lamellae orientation evolved with pressure increase and that the surface strain was correlated to the observed changes in lamellar orientation.

---

## 2. Material and methods

### 2.1. Cornea preparation

Investigations were performed in accordance with the tenets of the Declaration of Helsinki and the French legislation for scientific use of human corneas. Human corneas provided by the French Eye Bank (BFY, Paris, France) were unsuitable for transplantation and assigned to scientific use (E.E.B.A., 2010). For this study, we used 14 human corneas that exhibited endothelial cell densities between 1400 and 2750 cell/ $\text{mm}^2$  (mean value: 2330 cell/ $\text{mm}^2$ , higher than the viability threshold that is 2000 cell/ $\text{mm}^2$  (E.E.B.A., 2010)) (see Table 1). The corneas were stored at 31 °C in a storage medium (StemAlpha2 #7002, StemAlpha) until the day before the experiment. They were then immersed for 24 h in a deswelling medium (StemAlpha3 #7003, StemAlpha) to recover a thickness close to the physiological one. However, they were slightly edematous, with a mean thickness of 630  $\mu\text{m}$ , while the

**Table 1 – Clinical data of human corneas with the optical and mechanical analysis performed.**

BFY	Cornea #	Age	Gender	Endothelial cell density (cell/mm <sup>2</sup> )	Initial thickness (μm)	Optical analysis	Mechanical analysis
10167	1	83	F	1600	400	0–48 mbar	0–48 mbar
10375	2	68	M	–	680	–	0–48 mbar
10380	3	76	F	1400	580	0–48 mbar	–
10426	4	86	F	1850	700	0–48 mbar	0–48 mbar
10439	5	86	F	2750	500	0–48 mbar	–
10456	6	77	F	2750	600	0–48 mbar	–
10676	7	81	F	2650	550	0–64 mbar	0–48 mbar
10788	8	89	M	2600	650	0–64 mbar	0–64 mbar
10717	9	57	M	2500	900	0–64 mbar	0–64 mbar
10764	10	67	M	2700	650	0–64 mbar	–
10803	11	56	F	2500	650	0–64 mbar	0–64 mbar
10819	12	65	F	2700	650	0–64 mbar	0–64 mbar
10794	13	77	M	1800	500	0–64 mbar	0–64 mbar
10862	14	71	F	2500	550	0–64 mbar	–

physiological central corneal thickness is around 500 μm. The corneas were surrounded by a small remaining of sclera (typically 1 mm of width).

Fluorescent micro-beads (0.5 μm diameter) were deposited on the external surface of the cornea. After one minute, the excess of beads was rinsed with Hanks balanced salt solution before insertion of the cornea in the experimental set up.

## 2.2. Inflation system and loading path

The corneas were installed on a custom-built pressure chamber, designed to be placed under the nonlinear optical microscope (Fig. 1a and b). We attached the cornea to the chamber by gluing the sclera to the top part of the chamber and by gripping the sclera between the two parts of the chamber. This was generally enough to prevent leaks, which were detected by abnormal pressure temporal evolution. Pressure was continuously recorded in the chamber by a pressure sensor (STS ATM.23, range 0–100 mbar). The optical contact between the cornea and the water immersion microscope objective was maintained with an optical gel (Lacrigel, Europhtha).

We injected Hanks balanced salt solution in the chamber through a homemade injector, at constant debit (2 mm<sup>3</sup> s<sup>-1</sup>) up to the chosen pressure steps  $P_j$  (16, 32, 48 and 64 mbar). The injection was stopped during the image acquisition (imposing a constant volume under the cornea), and then Hanks solution was injected again until the next pressure level (see Fig. 1c for the loading path). These pauses were done to prevent cornea movements during imaging.

## 2.3. Polarization-resolved nonlinear optical microscopy

Nonlinear optical imaging was performed using a custom-built laser scanning upright microscope (Gusachenko et al., 2010; Latour et al., 2012b). The laser source was a femtosecond titanium:sapphire laser (Tsunami, SpectraPhysics) tuned to 860 nm and scanned within the sample to record two-dimensional pixel-wise images at increasing depths. High numerical aperture water immersion objective (20×, NA 0.95, Olympus) was used to achieve 0.4 × 1.6 μm<sup>2</sup> (respectively lateral and axial) resolutions near the sample surface.

The polarization state of the excitation beam was controlled by using two motorized achromatic waveplates inserted at the back pupil of the objective. The quarter waveplate controlled the polarization state (circular or linear) and the half waveplate was used to rotate the orientation of the linear polarization and acquire polarization-resolved SHG signals. Two-photon excited fluorescence (2PEF) signals were detected in the backward direction, while SHG signals were collected both in the backward (B-SHG) and in the forward directions (F-SHG) with appropriate filters (FF01-680/SP, FF01-720/SP, Semrock for laser excitation rejection, GG400, Schott for 2PEF signals and FF01-427/10, Semrock for SHG signals) (Fig. 1a). These signals were detected using photon-counting photomultiplier tubes (P25PC, Electron Tubes). Multimodal image stacks were recorded using 200–300 kHz pixel rate. Laser power at the objective focus was typically 20 mW at the sample surface and was increased with imaging depth until 140 mW.

## 2.4. Multiscale acquisition protocols

A volume of interest was selected off the geometric center of the cornea to observe larger strains (Fig. 1d) (Boyce et al., 2008). The typical distance between the center of the selected volume and the geometric center of the cornea varied between 0.5 and 1.1 mm (mean distance: 0.8 mm). Using conventional optical microscopy available on the same microscope, the geometric center was identified by its equidistance to the sclera along two perpendicular directions.

For each loading step, three types of stack were recorded as illustrated in Fig. 1d:

1. Stack #1 gave qualitative information (2PEF, F-SHG and B-SHG) on the corneal microstructure through the whole corneal thickness using circularly polarized excitation (512 × 512 μm<sup>2</sup> field of view, 0.8 μm pixel size, 20–50 μm axial steps). Acquisition time was about 1 min.
2. Stack #2 was recorded on the surface of the specimen to accurately locate the fluorescent beads from their 2PEF signals for further surface deformation characterization (512 × 512 μm<sup>2</sup> field of view, 0.53 μm pixel size, 1 μm axial steps). Acquisition time was 5–10 min.

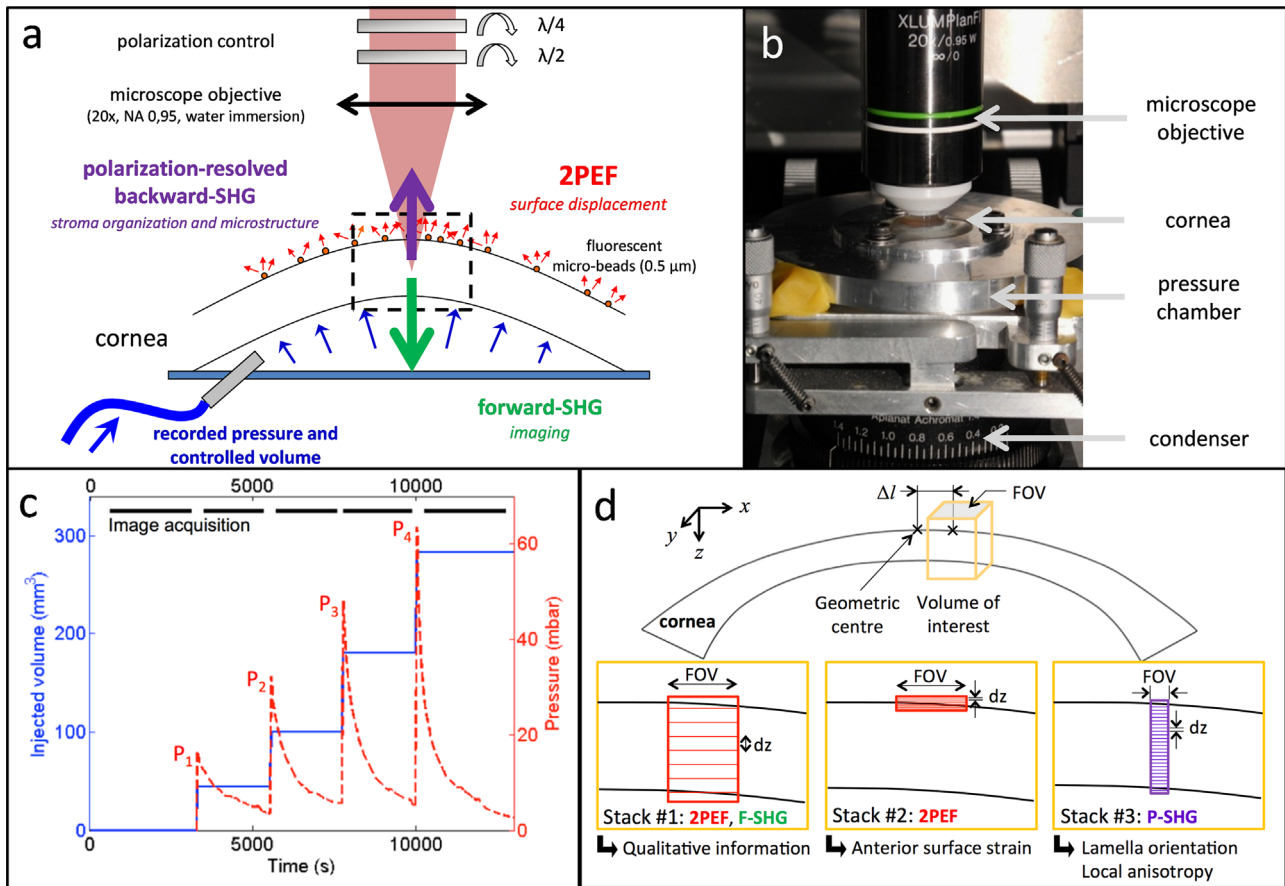


**Fig. 1 – Experimental set up.** (a) Laser scanning nonlinear optical microscope with rotating waveplates to control the polarization state of the excitation beam. The cornea, coated with fluorescent micro-beads ( $0.5 \mu\text{m}$  diameter), is placed in a pressure chamber, under the microscope objective. Forward-SHG (F-SHG) and backward-SHG (B-SHG) and 2PEF signals are simultaneously detected with appropriate spectral filters. Polarization-resolved SHG signals (P-SHG) are only acquired in the backward direction where they are more robust (see text) (b) Picture of the setup showing the pressure chamber inserted between the condenser and the microscope objective. (c) Mechanical loading path. Hanks balanced salt solution is injected until the recorded pressure reaches the chosen level  $P_j$ . During image acquisition, injected volume remains constant and recorded pressure decreases due to stress relaxation. (d) Image acquisition in an off-centered volume of interest. Stack #1 (2PEF and F-SHG, field of view (FOV) =  $512 \times 512 \mu\text{m}^2$ , z-step ( $dz$ ) =  $50 \mu\text{m}$ ) gives qualitative information about the cornea. Stack #2 (2PEF from micro-beads, FOV =  $512 \times 512 \mu\text{m}^2$ ,  $dz = 1 \mu\text{m}$ ) is used to determine surface displacement. Stack #3 (P-SHG, FOV =  $90 \times 150 \mu\text{m}^2$ ,  $dz = 3 \mu\text{m}$ , angular steps  $10^\circ$ ) is used to determine lamellae orientations and local anisotropy parameter.

3. Stack #3 was recorded using P-SHG (polarization-resolved B-SHG) signal to obtain quantitative information on the fibrillar collagen organization through the whole corneal thickness ( $160 \times 160 \mu\text{m}^2$  field of view,  $1.6 \mu\text{m}$  pixel size, 3–4  $\mu\text{m}$  axial steps, linearly polarized excitation from  $-90^\circ$  to  $+90^\circ$  with  $10^\circ$  angular steps). Acquisition time was 10–20 min depending on the corneal thickness and the chosen axial step.

P-SHG image processing was performed as already described in (Latour et al., 2012b). Briefly, SHG signals were averaged on regions of interest (ROI) of  $8 \times 8$  pixels ( $12.8 \times 12.8 \mu\text{m}^2$ ) and the resulting data were then fitted without any pre-processing using theoretically derived formulas for P-SHG data (Latour et al., 2012b). For each ROI, the orientation of the collagen fibrils (angle  $\varphi$ ) was obtained by fitting the data as the excitation polarization angle giving the

maximal SHG signal. The precision on the fibril orientation is better than  $1^\circ$  in our experimental conditions as demonstrated in (Teulon et al., 2015). Fitted P-SHG data also provided the anisotropy parameter  $\rho$  that was obtained as the square root of the ratio of the signals for polarization excitation parallel (resp. perpendicular) to the collagen fibrils:  $\rho = \sqrt{I_{\parallel}/I_{\perp}}$ . This anisotropy parameter has been shown to measure the local order within the focal volume: the smaller the degree of alignment of the collagen fibrils within lamellae, the larger the anisotropy parameter (Gusachenko et al., 2012). These quantitative parameters  $\varphi$  and  $\rho$  were considered as valid only for coefficient of determination  $R^2 > 0.7$ . Practically, low  $R^2$  were obtained when the ROI included the interface of two adjacent lamellae (Latour et al., 2012a, b), so that our  $R^2 > 0.7$  criterion limited the data to ROI within a single lamella, with aligned collagen fibrils and significant orientation.

## 2.5. Digital volume correlation

Tridimensional (3D) displacement field was extracted by tracking the pattern of the micro-beads on the 2PEF image (stack #2) through digital volume correlation (DVC) using CorrelManuV software (Bornert et al., 2004). The size of every analysis region was chosen equal to  $50 \times 50$  pixels ( $27 \times 27 \mu\text{m}^2$ ) in  $x$ - and  $y$ -directions and 10 pixels ( $10 \mu\text{m}$ ) along  $z$ -direction. When cornea was significantly tilted with respect to the horizontal optical cross-section, it could be reduced to  $30 \times 30 \times 8$  voxels ( $16 \times 16 \times 8 \mu\text{m}^3$ ). The analysis region size was chosen as a compromise between the accuracy of the measured displacement and the number of independent measurements covering the volume of interest, that-is-to-say using non-overlapping analysis regions.

The DVC analysis regions were initially distributed over the corneal surface to maximize the covered surface and limit their overlapping. The edges of the image were avoided because of artefacts. Some analysis regions were repositioned in case of abnormal displacement of the epithelium or low micro-beads density.

To estimate the accuracy of the measurement, DVC was first conducted between two stacks of the same zone recorded without any loading ( $P_0=0$  mbar) but after a small translation of the chamber.

## 2.6. Statistical analysis

Data of all loading steps between  $P_0=0$  mbar and  $P_4=48$  mbar were analyzed using GraphPad Prism (GraphPad Software, San Diego California). Analysis was not done for the step  $P_5=64$  mbar, due to the small number of corneas reaching this step (Table 1). All measurements on single cornea and error estimations are expressed as mean  $\pm$  Standard Deviation (SD). All statistical data on all corneas are expressed as mean  $\pm$  Standard Error (SE). The normal distribution of populations was assessed using Shapiro–Wilk normality test. Repeated measures one-way ANOVA with Tukey post-test (resp. Friedman test with Dunn's post-test) were performed for data observing (resp. not observing) a normal distribution. A  $p$ -value less than 0.05 was considered statistically significant.

## 3. Results

### 3.1. Polarization-resolved SHG characterization of the stroma

The corneal stroma that is mainly composed of type I fibrillar collagen, exhibited strong endogenous SHG signals as previously reported (Aptel et al., 2010; Han et al., 2005; Latour et al., 2012b; Matteini et al., 2009; Morishige et al., 2014; Winkler et al., 2013, 2015; Yeh et al., 2002). F-SHG images showed striated features that are generally attributed to the orientation of the nanometer scale collagen fibrils in the lamellae (Fig. 2a) (Latour et al., 2012b). These striated features showed no waviness, even at low-pressure, indicating that the slight edema of the cornea did not affect the lamellae organization. In contrast to F-SHG signals, backward SHG (B-

SHG) signals from the same area were spatially homogeneous, due to smaller coherence length (Fig. 2b) (Latour et al., 2012b). Polarization-resolved SHG was therefore performed on backward detected signals to take advantage of this smaller coherence length and obtain accurate quantitative information about the microstructure of the stroma.

We previously showed that P-SHG microscopy was a robust and effective technique to determine the orientation of nanometer-sized collagen fibrils in cornea (Latour et al., 2012b) (Fig. 2c). These collagen fibrils align to form collagen lamellae and, as previously demonstrated (Latour et al., 2012b), we considered that the orientation provided by P-SHG matched the one of the collagen fibrils within the collagen lamellae. We computed these orientations along the whole thickness of the corneal stroma to quantify the lamellae orientation probability (Fig. 2e). This histogram clearly exhibited two orthogonal peaks ( $\varphi_1$  and  $\varphi_2$ ) also observed in polar diagram (Fig. 2f). The number of lamellae oriented along these two peaks ( $\pm 15^\circ$ ) represented 60–70% of the total number of lamellae and the dominant orientation  $\varphi_1$ , further used to define the lamellae coordinate system for strain determination was defined as the center of the  $30^\circ$ -cone containing the most lamellae through whole corneal thickness. These results were consistent with X-ray scattering patterns reported in the literature (Hayes et al., 2007). Simultaneously, we measured the anisotropy parameter  $\rho$  from the same area (Fig. 2d) to get information about the degree of alignment of the collagen fibrils within lamellae (Latour et al., 2012b).

### 3.2. Corneal microstructure versus loading for one cornea

Corneal microstructure was characterized under increasing pressure by P-SHG. To have a better insight into the microstructure organization, the initial acquired volume was divided into three parts of equal thickness along corneal depth. Fig. 3a shows the lamellae orientation probability in the whole stromal thickness (*in gray*) and in the anterior (*in blue*), middle (*in red*) and posterior (*in green*) stroma for cornea #13, which is representative of the typical behavior observed in this study. The two orthogonal main orientations were present at each depth, and they remained constant when intra-ocular pressure increased.

We quantified the proportion of collagen lamellae oriented along the main direction  $\varphi_1 \pm 15^\circ$  (Fig. 3b) and along the orthogonal direction  $\varphi_2 \pm 15^\circ$  (Fig. 3c), for each pressure step. At each step, the very same volume of interest was observed by retrieving the pattern of the fluorescent beads at the surface.

The proportion of lamellae in the stroma along the main peak decreased with pressure while the one along the second orthogonal peak increased with pressure (*gray bars* in Fig. 3b and c). More specifically, we observed a decrease (resp. increase) of the number of collagen lamellae oriented along the main (resp. perpendicular) direction with the pressure for the middle and posterior parts (*red and green bars* in Fig. 3b and c), while the more isotropic organization of the lamellae in the anterior part was maintained (*blue bars*).

The local anisotropy parameter  $\rho$ , related to the local organization within lamellae, was also quantified for each

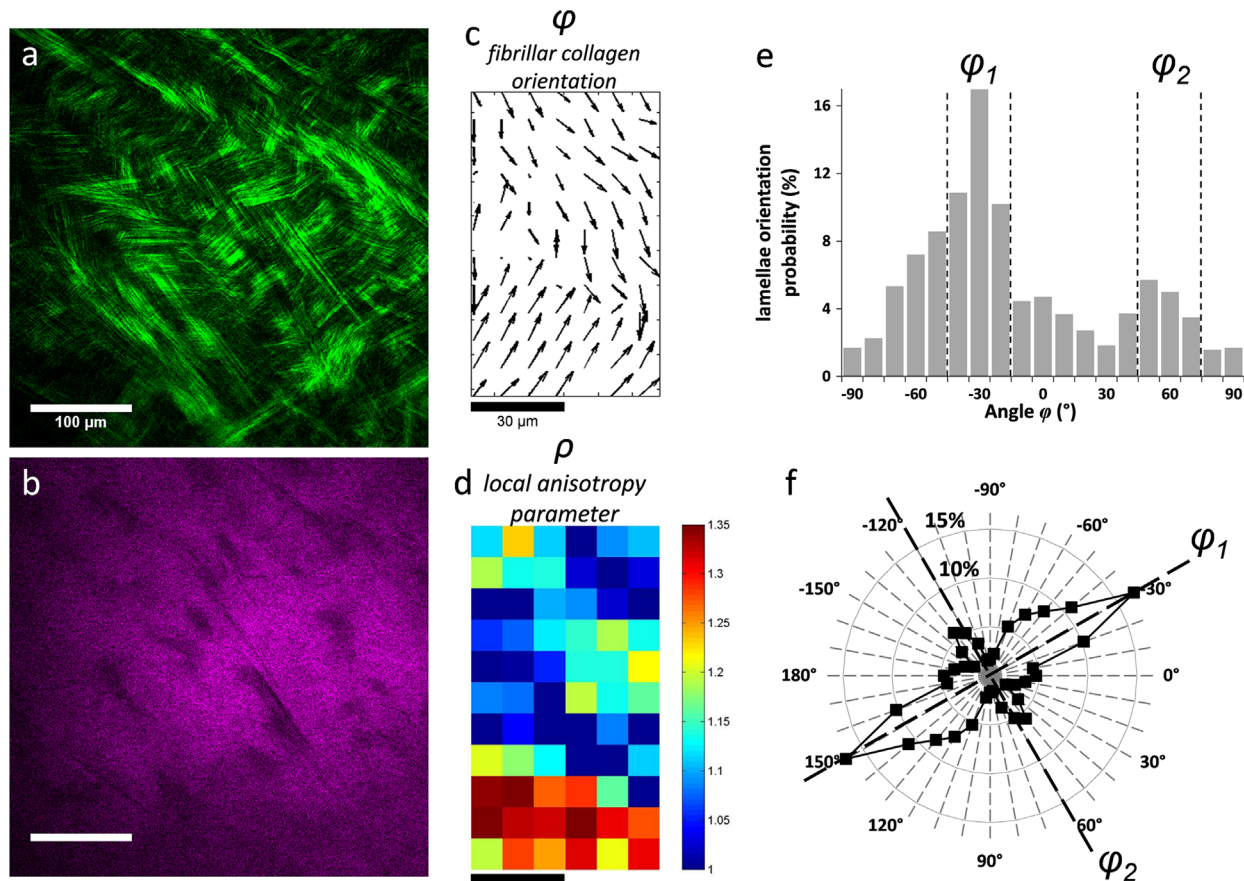


**Fig. 2** – Polarization-resolved SHG (P-SHG) imaging on cornea #7. (a) F-SHG (green) and (b) B-SHG (magenta) images of the stroma at 400  $\mu\text{m}$  deep, with no polarization resolution. Mappings of (c) the orientation of the collagen fibrils  $\varphi$  represented with arrows and (d) the local anisotropy parameter  $\rho$  determined from P-SHG signals obtained from the same area ( $90 \times 150 \mu\text{m}^2$ ) at 300  $\mu\text{m}$  depth within the stroma. (e) Histogram and (f) polar diagram of the lamellae orientation probability on the whole corneal thickness. Two preferential orthogonal orientations were observed  $\varphi_1$  and  $\varphi_2$ . Scale bars: (a and b) 100  $\mu\text{m}$  and (c and d) 30  $\mu\text{m}$ . (For interpretation of the references to color in this figure legend, the reader is referred to the web version of this article.)

loading step and the average values were calculated on the whole thickness.  $\rho$  values did not vary versus depth (data not shown); a slight increase was observed during the experiment (Fig. 3d).

### 3.3. Statistical analysis of corneal microstructure evolution versus loading

The previous analyses were performed for all corneas. The summary of the corneal microstructure evolution is presented in Fig. 4. For all corneas, the proportion of collagen lamellae along the direction  $\varphi_1 \pm 15^\circ$  (resp.  $\varphi_2 \pm 15^\circ$ ) decreased (resp. increased) with increasing pressure in the middle and posterior parts (Fig. 4a and b). In the anterior part, the proportion of lamellae did not significantly change, due to the more isotropic organization of the collagen lamellae in this region of the stroma. This behavior was emphasized by computing the ratio of collagen lamellae along directions  $\varphi_1 \pm 15^\circ$  and  $\varphi_2 \pm 15^\circ$  (Fig. 4c). This ratio increased with pressure, showing a reorganization of the stroma toward a balancing of the numbers of lamellae in the two main directions.

For all corneas, the local anisotropy parameter  $\rho$  was calculated and averaged along the whole thickness of corneas at each loading step (Fig. 4d). A slight increase was observed, which meant that the disorder increased slightly at sub-micrometer scale. It was tightly related to the evolution of the corneal thickness, which was measured at each pressure step by use of stack #1 (Fig. 4e). During our quite long experiments, the corneas became edematous probably impairing the well-aligned organization of the collagen fibrils within the lamellae.

### 3.4. Strain determination

A post-processing procedure combining DVC and strain analysis was applied on 2PEF images of the micro-beads (stack #2) to quantify corneal anterior surface strains, as illustrated in Fig. 5. Micro-beads were spread all over the corneal anterior surface included in the volume of interest, providing variations of the fluorescence signal recorded in stack #2. Fig. 5a shows the maximum intensity projection on x-y plane of this fluorescence signal, which is represented in red. Fig. 5a also shows a typical distribution of the analysis

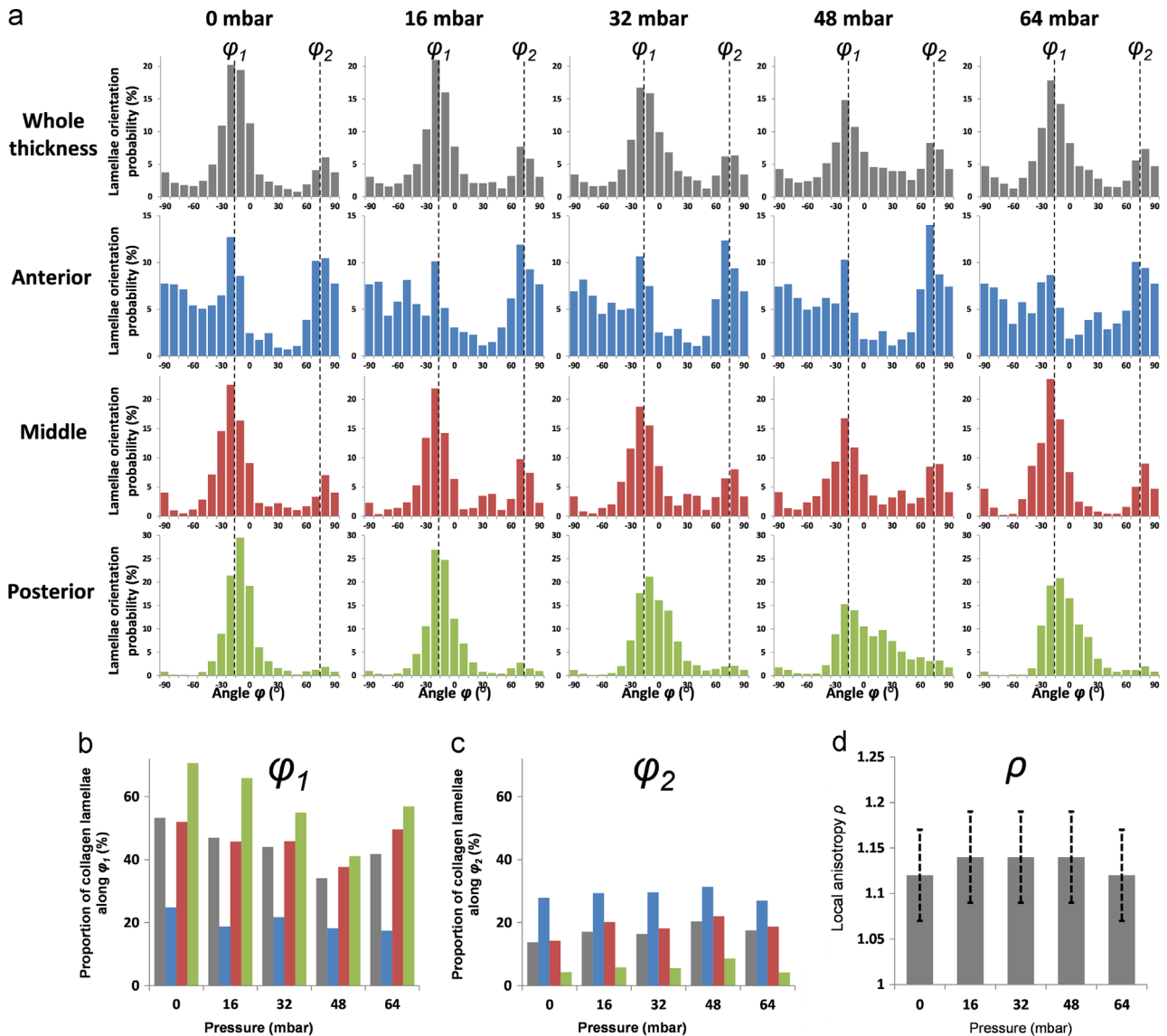


**Fig. 3 – Corneal micro-structure versus loading on cornea #13. (a) Histogram of collagen lamellae orientation probability versus the loading steps (0, 16, 32, 48 and 64 mbar) for the whole thickness (gray), the anterior (blue), middle (red) and posterior parts (green) of the cornea. The orthogonal preferential orientations ( $\phi_1, \phi_2$ ) are shown with dashed lines. Evolution of the proportion of collagen lamellae along (b) the main orientation  $\phi_1 \pm 15^\circ$  and (c) the orthogonal one  $\phi_2 \pm 15^\circ$  with the loading steps. (d) Evolution of the local anisotropy parameter  $\rho$  with the loading steps. Error bars correspond to SD. (For interpretation of the references to color in this figure legend, the reader is referred to the web version of this article.)**

regions (white squares) over the field of view. Using DVC, the displacement of the analysis regions was calculated in 3D. A 2D mesh was created using Delaunay triangulation to connect the analysis regions' centers and imported in Abaqus software using S3 shell elements. For each loading step, the measured displacement of every node was applied as new boundary conditions.

A lamellae coordinate system was defined from P-SHG analysis: axes 1 and 2 corresponded to the previously identified dominant orientations  $\phi_1$  and  $\phi_2$  while axis 3 was the cross-product of axes 1 and 2. The displacement of the anterior surface of the cornea was visualized in this lamellae coordinate system (Fig. 5b) and local strains were evaluated in every element to calculate the strain distribution over the

zone of interest. We observed a high dispersion in the local strain distribution (Fig. 5c) related to the positioning error of each node. To improve the accuracy of the results, a mesoscopic strain (Fig. 5d), representative of an average strain of the zone of interest, was defined for each loading step as follows:

- Since the field of view was only 0.5 mm wide, the corneal surface was approximated by a median plane identified using least-squares method between the analysis regions' centers. The mean angle between the median plane and the x-y plane was  $5.2 \pm 3.3^\circ$  for all corneas (maximum value  $15.1^\circ$ ).

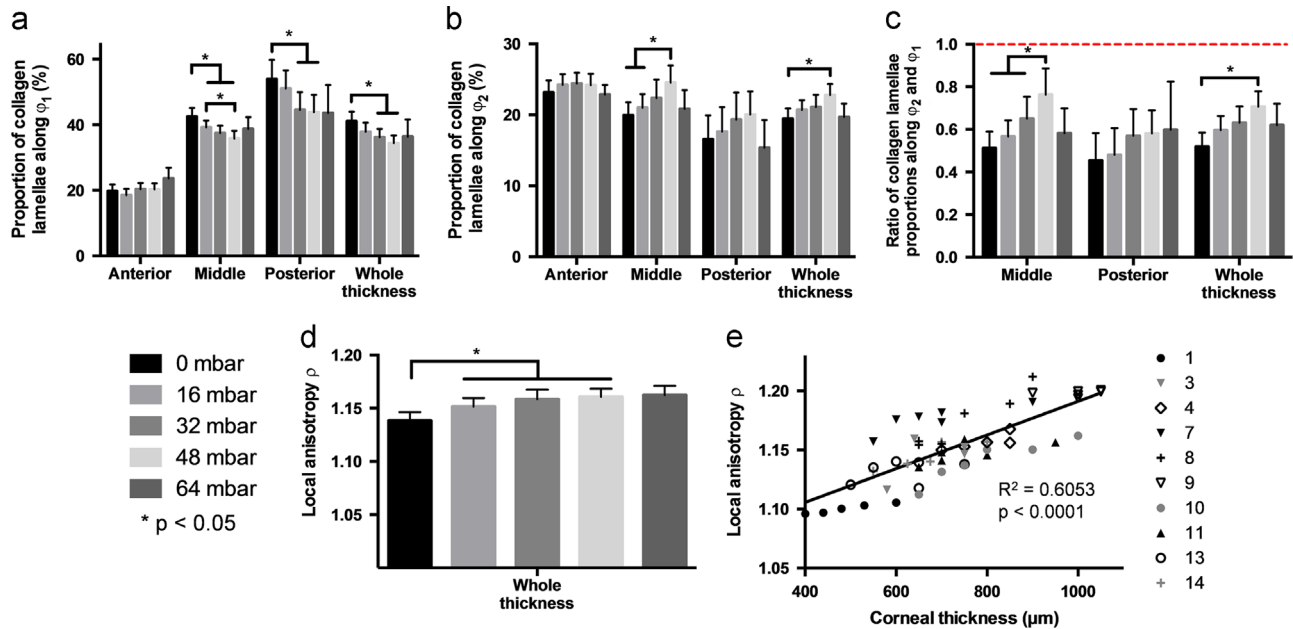


**Fig. 4 – Corneal micro-structure evolution.** (a and b) Evolution of the proportion of collagen lamellae along (a) the dominant orientation  $\varphi_1 \pm 15^\circ$  and (b) the orthogonal dominant orientation  $\varphi_2 \pm 15^\circ$  with the loading steps for all the studied corneas (Table 1) considering anterior, middle, posterior stroma and whole thickness of the tissue. (c) Same for the ratio of collagen lamellae proportion along  $\varphi_1 \pm 15^\circ$  and  $\varphi_2 \pm 15^\circ$ . (d) Same for the local anisotropy  $\rho$  on the whole thickness. Error bars correspond to SE and \* means that  $p < 0.05$  using Tukey or Dunn's post-test. (e) Evolution of the local anisotropy parameter  $\rho$  with the corneal thickness for all the studied corneas. Using an  $F$  test, the reported  $p$ -value tested the null hypothesis that the overall slope was zero.

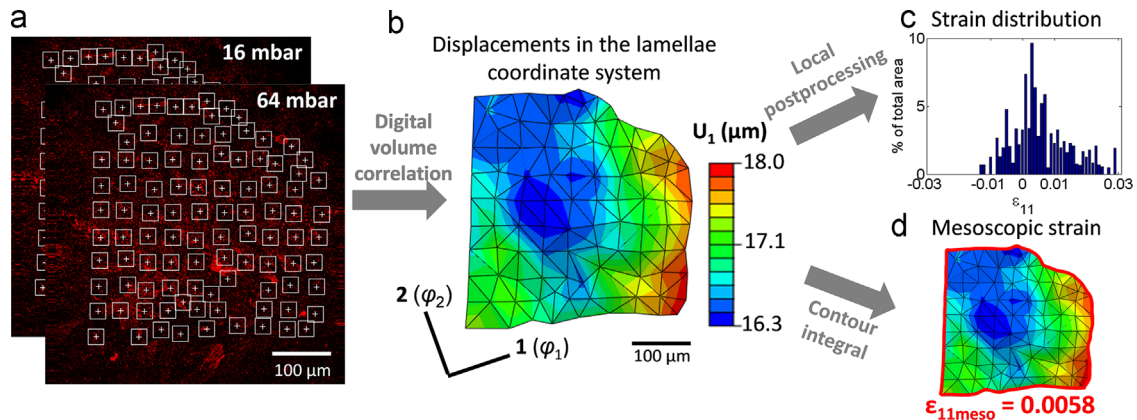


**Fig. 5 – Mechanical post-processing.** (a) Digital volume correlation was used on detailed 2PEF imaging of the micro-beads (stack #2) to calculate the 3D-displacement of the corneal surface between two loading steps. Pictures are maximum intensity projections of 2PEF acquisitions along the  $z$ -axis. White squares represent the analysis regions and white dots their centers. (b) Visualization of the displacement in the coordinate system defined by the two dominant orthogonal orientations ( $\varphi_1$ ,  $\varphi_2$ ) of the collagen lamellae obtained from P-SHG data. (c) Distribution of the normal strain along  $\varphi_1$  measured in every element. (d) Calculation of the mesoscopic strain of the zone of interest, defined by integration of the displacement along its contour. Scale bars: 100  $\mu\text{m}$ . (For interpretation of the references to color in this figure, the reader is referred to the web version of this article.)

- The displacements, measured between the reference step and the analyzed step, were projected on this plane, axes 1 and 2 still corresponding to dominant orientations  $\varphi_1$  and  $\varphi_2$ .
- The mesoscopic deformation gradient tensor  $F$  was calculated by integration of the projected displacements along the edges of the zone of interest.

- The strain tensor was then defined, under the small perturbation hypothesis, by  $\epsilon_{\text{meso}} = 1/2 (F^T + F)$  and considered as the surface strain of the region of interest.

This mesoscopic strain was less sensitive to the displacement noise since at least 20 nodes, distributed on the edges of the volume of interest, were used to compute it.

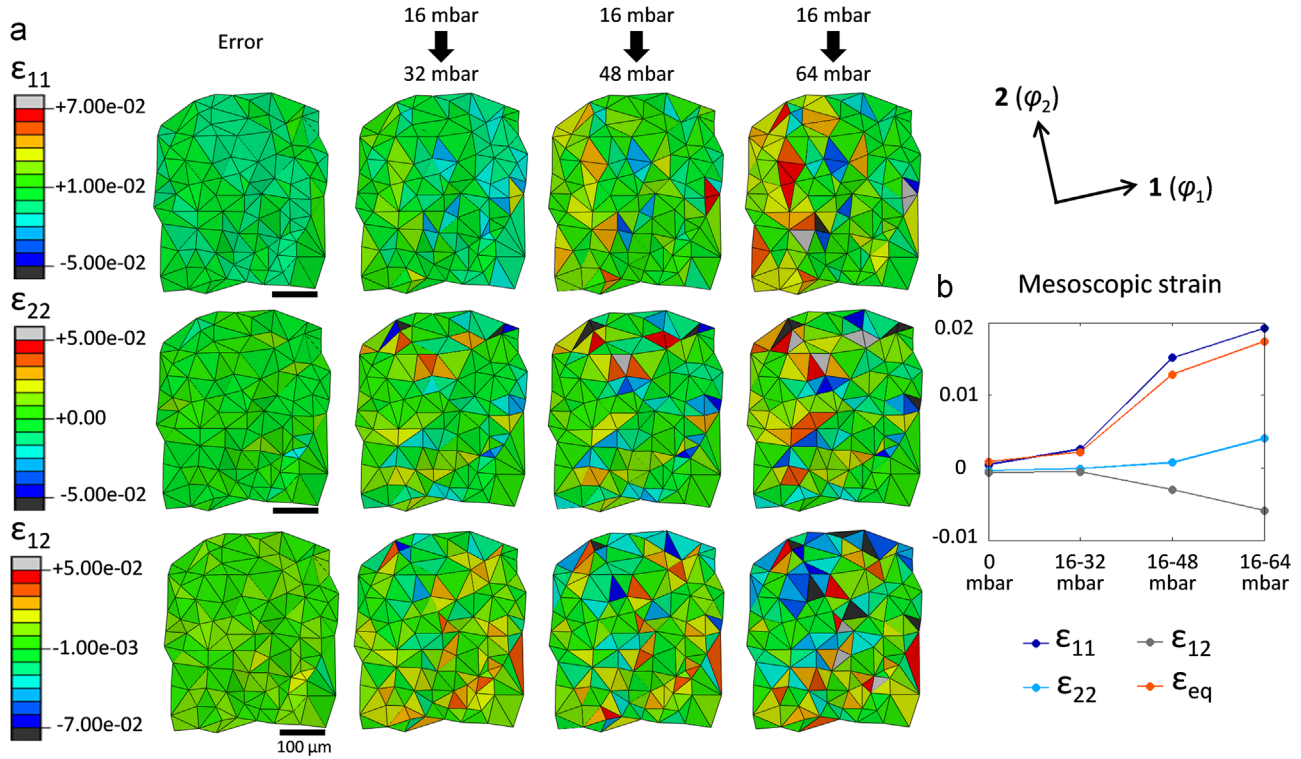


**Fig. 6 – Corneal surface strains versus loading on cornea #13. (a) Strain maps along directions 11 (preferential orientation  $\varphi_1$ ), 22 (preferential orientation  $\varphi_2$ ) and 12, for each loading step,  $P_1=16$  mbar being considered as reference. Error is the strain calculated between two images acquired sequentially before inflation of the cornea ( $P_0=0$  mbar). (b) The equivalent strain, defined as  $\epsilon_{eq} = 2/3(\epsilon_{11}^2 + \epsilon_{22}^2 + 2\epsilon_{12}^2)$ , and the three components of the mesoscopic strain of the zone of interest versus the loading steps. Scale bars: 100  $\mu\text{m}$ . (For interpretation of the references to color in this figure, the reader is referred to the web version of this article.)**

### 3.5. Surface strain evolution versus loading for one cornea

We measured the evolution of the surface strain distributions corresponding to the volume of interest versus increasing pressures for all corneas. The results obtained for cornea #13 are displayed in Fig. 6. The first loading step,  $P_1$ , was chosen as reference since large displacements were observed between  $P_0=0$  mbar and  $P_1=16$  mbar, due to corneal edges repositioning in the experimental set up at first loading. The same post-processing was performed between two images acquired sequentially before inflation of the cornea to evaluate the measurement error without any loading but after a small translation of the chamber (column 1 in Fig. 6a). These error strains were representative of inaccuracies related to image acquisition, micro-bead fixation and DVC, and reached 1% in some elements. Normal strain maps (lines 1 and 2 in Fig. 6a) showed the progressive stretching of cornea #13 along dominant orientations  $\varphi_1$  and  $\varphi_2$  between the first loading step at  $P_1=16$  mbar and the following loading steps ( $P_2=32$  mbar,  $P_3=48$  mbar,  $P_4=64$  mbar in columns 2–4 respectively). Shear strain map (line 3) showed similarly the progressive shearing of the corneal surface. Due to the large uncertainties, we could not directly use the local measurements and therefore focused on the less noisy mesoscopic strain (Fig. 6b). Apart from poorly positioned nodes, the strain seemed rather uniform, meaning that the deformation

was likely to be homogeneous at the hundreds of micrometers scale.

For cornea #13, components 11 and 22 of the mesoscopic strain increased during inflation (Fig. 6b). A larger increase was observed for component 11, revealing more elongation along main orientation  $\varphi_1$  in comparison with elongation along  $\varphi_2$ . Component 12 slightly decreased toward negative values but its evolution was minor compared to the evolution of the normal strains. This behavior was generally observed for all corneas.

An equivalent strain was defined by the following equation:

$$\epsilon_{eq} = \sqrt{\frac{2}{3}(\epsilon_{11}^2 + \epsilon_{22}^2 + 2\epsilon_{12}^2)}.$$

This variable, always positive, was representative of the general state of strain. For cornea #13,  $\epsilon_{eq}$  increased similarly to  $\epsilon_{11}$  with loading, but, generally, the equivalent strain increase was more pronounced as a result of the combined increase of components 11 and 22.

### 3.6. Statistical analysis of the surface strain evolution versus loading

Fig. 7 shows the mean and the SE of the normal ( $\epsilon_{11}$  and  $\epsilon_{22}$ ), shear ( $\epsilon_{12}$ ) and equivalent ( $\epsilon_{eq}$ ) surface mesoscopic strains for each loading step for all studied corneas. Regarding error

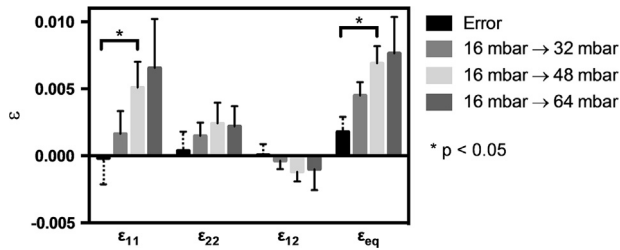


**Fig. 7 – Corneal surface mesoscopic strains.** Mean and SE (solid error bars) of the mesoscopic strains along directions 11, 22 and 12 and of the equivalent strain for each loading step for all studied corneas (Table 1). Mean and SD (dotted error bars) for error estimations. A  $p$ -value  $< 0.05$  using Tukey or Dunn's post-test was chosen for statistical significance.

estimation (black columns with dotted error bars in Fig. 7), the mean and the SD are displayed for all the components of the error mesoscopic strains measured between two successive image acquisitions with no additional mechanical loading. For components 11, 22 and 12, the mean of the error strains represents the accuracy (i.e. repeatability) of the results whereas the error bar calculated as the standard deviation represents the precision of the measurement. As the equivalent strain is always positive, the mean of the calculated error equivalent strains represents the precision of the measurements.

Despite the large dispersion of the results, we measured a significant increase of  $\varepsilon_{11}$  and  $\varepsilon_{eq}$  strains between 16 and 48 mbar, larger than the measured noise. This confirmed the increasing trend observed for both variables on each individual cornea. Similar trend was observed for  $\varepsilon_{22}$  and  $\varepsilon_{12}$  but our number of samples was not large enough to reach a statistically significant difference. Regarding normal strains,  $\varepsilon_{11}$  was generally higher than  $\varepsilon_{22}$  but the difference was not statistically significant at 48 mbar.

### 3.7. Correlation between microstructure reorganization and mechanical loading

The proportion  $\frac{\Delta N_{\varphi_i}}{N_{\varphi_i}}$  of lamellae that aligned within  $15^\circ$  either side of the dominant orientations  $\varphi_i$  ( $i=1,2$ ) during loading ( $P_1=16$  mbar to  $P_3=48$  mbar) was defined by the following equation:

$$\frac{\Delta N_{\varphi_i}}{N_{\varphi_i}} = \frac{N_{\varphi_i}(P_3=48 \text{ mbar}) - N_{\varphi_i}(P_1=16 \text{ mbar})}{N_{\varphi_i}(P_1=16 \text{ mbar})}$$

with  $N_{\varphi_i}(P_j)$  the number of lamellae oriented along direction  $\varphi_i \pm 15^\circ$  at loading step  $P_j$ .

A higher (resp. lower) density of collagen fibrils along direction  $\varphi_i \pm 15^\circ$  for  $P_3=48$  mbar corresponded to  $\Delta N_{\varphi_i}/N_{\varphi_i}$  positive (resp. negative). In Fig. 8,  $\Delta N_{\varphi_i}/N_{\varphi_i}$  was plotted as a function of the observed normal strain  $\varepsilon_{ii}$  along direction  $\varphi_i$ . A significant correlation was observed between the reorientation of the lamellae and the normal strain: when the collagen fibril density increased (resp. decreased) along one direction, a smaller (resp. larger) elongation was observed on the anterior surface of the cornea. Microstructural reorganization was then observed in the volume, mostly in the two posterior thirds of corneas, whereas strains were measured on their

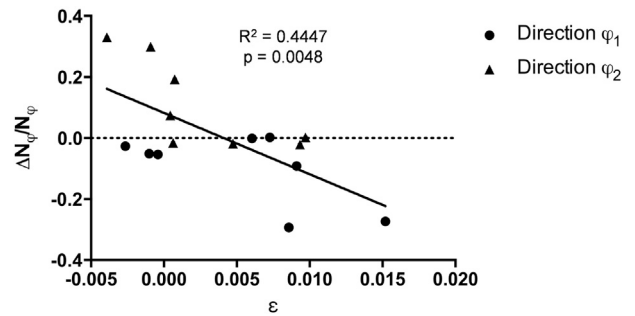


**Fig. 8 – Correlation between proportion of reoriented lamellae and mesoscopic strain from 16 mbar to 48 mbar for all corneas.** Data along the direction  $\varphi_1$  (resp.  $\varphi_2$ ) are represented by circles (resp. triangles). The proportion of reoriented lamellae is calculated in the whole thickness of the cornea (see text). Black line corresponds to a linear regression. Using an  $F$  test, the reported  $p$ -value tested the null hypothesis that the overall slope was zero.

anterior surface. However, using current technologies, strains could not be measured in the corresponding volume without affecting the mechanical behavior of the stroma (by sectioning or markers insertion).

## 4. Discussion

Biomechanical studies of cornea have focused on the link between the microstructure of the collagen lamellae and the mechanical properties, to better understand structural pathologies and to help laser surgery. However, they have been impeded by technical difficulties in obtaining information on the corneal microstructure without damaging the tissue. Techniques such as scanning electron microscopy (SEM) (Radner et al., 1998) and X-ray scattering from Synchrotron radiation (Meek and Boote, 2009) require tissue fixation, and even sectioning for electron microscopy, preventing any follow-up of the organization on fresh tissues. In this study, we used P-SHG microscopy to overcome these technical limitations, since this optical method is applicable in intact fresh tissue and does not require any staining. By combining P-SHG with an inflation test, we were able for the first time to our knowledge to investigate the reorganization of the collagen lamellae at increasing pressure in the same cornea.

Previous works using SEM and X-rays have demonstrated that collagen lamellae are mainly oriented along two orthogonal directions in human corneas. SEM results were obtained on slices cut at different selected depths along the stroma (Radner et al., 1998) and X-ray results were averaged orientations on the whole thickness (Meek and Boote, 2009). By using P-SHG microscopy, we quantitatively determined the orientation of the collagen lamellae at each depth within the tissue thanks to the intrinsic optical sectioning of this nonlinear optical mode of contrast. Orientation probability was then obtained by computing all these orientations within the whole corneal thickness or in specific volumes of interest. On the whole thickness, we measured two orthogonal preferential orientations attributed to the nasal-temporal and inferior-superior directions (Hayes et al., 2007). As a further

characterization, we showed that this organization was found in the middle and posterior parts whereas, in the anterior part, collagen lamellae were isotropically organized. Note that the whole thickness lamellae organization deduced from X-ray diffraction measurements showed an isotropic component beside the oriented one. This isotropic component was less present in our SHG measurements and further correlative measurements on same corneas would be of great interest to explain such a difference.

Mechanical measurements reported by Hjortdal (Hjortdal, 1995, 1996; Hjortdal and Jensen, 1995) and Shin et al. (1997) were obtained using particle tracking on the epithelial side of corneas subjected to increased IOP, as in our study, and therefore deserve a comparison with our results. These groups divided the cornea into different regions (center, para-center, periphery and limbus) to evaluate regional mechanical properties. The zone of interest in our study was located between the center and the para-center zone. The levels of strain measured here were slightly higher than Hjortdal finding for normo-hydrated corneas (Hjortdal, 1995, 1996) but were in good agreement with strains measured by Hjortdal in swollen corneas (Hjortdal and Jensen, 1995) and by Shin on normo-hydrated corneas (Shin et al., 1997). The standard deviation of the measurements for all corneas was in good agreement with the one obtained by Shin et al. (1997). Several factors led to this high-standard deviation such as the small size of the zone of interest ( $450 \times 450 \mu\text{m}^2$ ), the progressive crimping of the epithelium and the migration of the micro-beads inside the epithelium. Hjortdal noticed in the para-center zone that circumferential strain was significantly higher than meridional strain. This is consistent with the difference observed here between normal strains measured along dominant orientations  $\varphi_1$  and  $\varphi_2$ , although this difference was not statistically significant.

In our experiments, the measured strain showed no correlation with the initial distribution of collagen lamellae orientations. With increasing IOP, elongation of the cornea along the first dominant orientation  $\varphi_1$  was larger than along the second dominant orientation  $\varphi_2$  whereas lamellae oriented along  $\varphi_1 \pm 15^\circ$  were almost twice more numerous than lamellae oriented along  $\varphi_2 \pm 15^\circ$ . Hence, at the scale of our field of view and for IOP variations close to physiological ranges, cornea appeared more rigid along the direction involving less aligned collagen fibrils. This observation is inconsistent with numerous studies that attributed stromal stiffness to the orientation and the density of collagen fibrils only (Nguyen and Boyce, 2011; Pandolfi and Vasta, 2012; Petsche and Pinsky, 2013; Pinsky et al., 2005; Studer et al., 2010; Whitford et al., 2015). However, since the measured difference was not statistically significant, this observation may result from experimental artefacts. Recent studies showed also that other parameters, which were not quantified here, such as lamellae inclination relative to Bowman's layer (Abass et al., 2015; Cheng et al., 2015; Morishige et al., 2014) and lamellar interweaving (Winkler et al., 2015) contributed to stroma mechanical behavior. Since strains were measured locally and on the anterior surface of the cornea, the way lamellae inserted into Bowman's layer and connected to each other may significantly affect the measured strain. Indeed, if locally, lamellae oriented within  $15^\circ$  either

side of direction  $\varphi_2$  were more involved in branching, the rigidity along this direction would be increased.

Moreover, microstructure reorganized with increasing pressure, especially in posterior and mid-stroma. We observed an inverse correlation between the surface elongation and the proportion of lamellae reoriented during loading along the same direction  $\varphi_i$ . In response to increased IOP, some lamellae, which were within  $15^\circ$  either side of dominant orientation  $\varphi_1$ , rotated to deviate from this direction  $\varphi_1$ . Conversely, other lamellae rotated to align with the orthogonal direction  $\varphi_2 \pm 15^\circ$ . To resist loading, more (resp. less) collagen fibrils were progressively mobilized along direction  $\varphi_2$  (resp.  $\varphi_1$ ), thus inducing a lower (resp. higher) surface elongation along this direction. This reorganization occurred mainly in posterior and mid-stroma, which are composed of large lamellae with limited connectivity, and mostly parallel to the corneal surface (Winkler et al., 2013). Two mechanisms could explain the observed lamellae reorientation under increasing pressure: lamellae could be sliding past each other when pressure increased or they could be simply deformed by the motion. Strain measurements inside corneal tissue would be necessary to identify the exact mechanism. However, using current technologies, such measurements would require markers or slicing of the tissue, which would modify its mechanical behavior. Swelling of the tissue may also contribute to lamella reorientation. However, between the loading steps at 16 and 48 mbar, swelling was limited to  $14 \pm 7\%$  of initial corneal thickness and no correlation was identified between corneal thickness variation and lamella reorientation (Supplementary material). Thus, the impact of swelling on reorganization was considered as secondary.

We also probed the nanometric organization of the collagen fibrils within the lamellae. Indeed, P-SHG microscopy is sensitive to optical anisotropy within the focal volume, through the anisotropy parameter  $\rho$ . It therefore enabled the determination of the degree of alignment of the 35 nm diameter collagen fibrils in the lamellae, although these fibrils were not optically resolved. The increase of the anisotropy parameter  $\rho$  was attributed to a lesser alignment of the collagen fibrils within the lamellae during the experiment (Gusachenko et al., 2012). We observed that this increase was associated to an increase of the cornea thickness (Fig. 4). Indeed, cornea became edematous during the loading experiment, probably due to the Hanks balanced salt solution injected in the pressure chamber under the cornea. It has been shown using transmission electron microscopy that stromal edema was associated with collagen fibril misalignment within lamellae (Plamann et al., 2010) and with modification of the interfibrillar distance. We therefore attributed the evolution of the local anisotropy parameter mainly to the edema within the corneal stroma that impaired the well-aligned organization of the collagen fibrils, rather than to the increasing IOP.

Finally, the stroma microstructure appeared to be modified by increased IOP. Lamellae from posterior and mid-stroma presented initially two orthogonal preferential orientations, with a first clearly dominant orientation. While IOP increased, these collagen lamellae slid and slightly rotated relative to each other toward balancing the proportions of lamellae oriented along the two preferential orientations. The

collagen organization within each lamella was kept intact, except for the small disorder introduced by the edema related to the duration of the experiment. Therefore, the stroma microstructure adapted to the increased IOP toward an equibiaxial microstructure, more resistant to the loading conditions. These new observations of non-elastic evolution of the lamellae distribution could lead to an improvement of the recent biomechanical models, which rely presently only on the initial distribution of lamellae orientation to predict the behavior of cornea during inflation (Petsche and Pinsky, 2013; Studer et al., 2010; Whitford et al., 2015) assuming a purely elastic evolution.

## 5. Conclusion

To our knowledge, we presented the first experimental investigation of the relationship between collagen lamellae orientation and surface strain in human corneas. We simultaneously carried out nonlinear optical microscopy imaging for structural characterization of the tissue and loading assays to mimic IOP variations. We showed that the 3D architecture of the stroma varied with depth, with less preferentially oriented lamellae in the anterior part, while deeper lamellae were organized along two orthogonal preferential orientations. We obtained clues about the relationship between the microstructure of the corneal stroma and the mechanical properties of this tissue. We showed that it was not the initial lamellae distribution but its evolution that was correlated to the surface strain. This effect should be incorporated in future biomechanical models of human cornea to help further understanding of ocular pathologies such as keratoconus (distorted corneal shape) and glaucoma, where intraocular pressure can reach, for long periods, the maximum level applied in this study. It should also improve develop optimized protocols for corneal graft surgery.

## Acknowledgments

The authors thank I. Sourati, S. Gleize and P. Sabatier from the “Banque Française des Yeux” for providing the human cornea buttons for scientific use. Gaël Latour was supported by “Bourse Berthe Fouassier-Fondation de France- Engt 2010 – 17488 and Aurélie Benoit was supported by the “Fédération Francilienne de Mécanique - Coup de Pouce 2011”.

## Appendix A. Supplementary material

Supplementary data associated with this article can be found in the online version at <http://dx.doi.org/10.1016/j.jmbbm.2015.12.031>.

## REFERENCES

- Abass, A., Hayes, S., White, N., Sorensen, T., Meek, K.M., 2015. Transverse depth-dependent changes in corneal collagen lamellar orientation and distribution. *J. R. Soc. Interface* 12, 20140717.
- Aptel, F., Olivier, N., Deniset-Besseau, A., Legeais, J.M., Plamann, K., Schanne-Klein, M.C., Beaurepaire, E., 2010. Multimodal nonlinear imaging of the human cornea. *Investig. Ophthalmol. Vis. Sci.* 51, 2459–2465.
- Beuerman, R.W., Pedroza, L., 1996. Ultrastructure of the human cornea. *Microsc. Res. Tech.* 33, 320–335.
- Bornert, M., Chaix, J.-M., Doumalin, P., Dupré, J.-C., Fournel, T., Jeulin, D., Maire, E., Moreaud, M., Moulinec, H., 2004. Mesure tridimensionnelle de champs cinématiques par imagerie volumique pour l'analyse des matériaux et des structures. *Instrumentation, Measure, Métrologie* 4, pp. 43–88.
- Boyce, B.L., Grazier, J.M., Jones, R.E., Nguyen, T.D., 2008. Full-field deformation of bovine cornea under constrained inflation conditions. *Biomaterials* 29, 3896–3904.
- Cheng, X., Petsche, S.J., Pinsky, P.M., 2015. A structural model for the in vivo human cornea including collagen–swelling interaction. *J. R. Soc. Interface*, 12, Article number: 20150241.
- Daxer, A., Fratzl, P., 1997. Collagen fibril orientation in the human corneal stroma and its implication in keratoconus. *Investig. Ophthalmol. Vis. Sci.* 38, 121–129.
- E.E.B.A., 2010. European Eye Bank Association Directory, 18th ed.
- Elsheikh, A., Geraghty, B., Rama, P., Campanelli, M., Meek, K.M., 2010. Characterization of age-related variation in corneal biomechanical properties. *J. R. Soc. Interface* 7, 1475–1485.
- Elsheikh, A., Ross, S., Alhasso, D., Rama, P., 2009. Numerical study of the effect of corneal layered structure on ocular biomechanics. *Curr. Eye Res.* 34, 26–35.
- Elsheikh, A., Wang, D., Pye, D., 2007. Determination of the modulus of elasticity of the human cornea. *J. Refract. Surg.* 23, 808–818.
- Gusachenko, I., Latour, G., Schanne-Klein, M.C., 2010. Polarization-resolved second harmonic microscopy in anisotropic thick tissues. *Opt. Express* 18, 19339–19352.
- Gusachenko, I., Viet, T., Goulam Houssen, Y., Allain, J.-M., Schanne-Klein, M.-C., 2012. Polarization-resolved second-harmonic generation in tendon upon mechanical stretching. *Biophys. J.* 102, 2220–2229.
- Han, M., Giese, G., Bille, J.F., 2005. Second harmonic generation imaging of collagen fibrils in cornea and sclera. *Opt. Express* 13, 5791–5797.
- Hayes, S., Boote, C., Lewis, J., Sheppard, J., Abahussin, M., Quantock, A.J., Purslow, C., Votruba, M., Meek, K.M., 2007. Comparative study of fibrillar collagen arrangement in the corneas of primates and other mammals. *Anat. Rec.* 290, 1542–1550.
- Hjortdal, J.O., 1995. Extensibility of the normo-hydrated human cornea. *Acta Ophthalmol. Scand.* 73, 12–17.
- Hjortdal, J.O., 1996. Regional elastic performance of the human cornea. *J. Biomech.* 29, 931–942.
- Hjortdal, J.O., Jensen, P.K., 1995. In-vitro measurement of corneal strain, thickness, and curvature using digital image-processing. *Acta Ophthalmol. Scand.* 73, 5–11.
- Krachmer, J.H., Mannis, M.J., Holland, E.J., 2005. *Cornea* 2nd edition ed.
- Latour, G., Gusachenko, I., Kowalczyk, L., Lamarre, I., Schanne-Klein, M.-C., 2012a. In vivo multiphoton imaging of the cornea: polarization-resolved second harmonic generation from stromal collagen. In: *Proceedings of SPIE 8226 – Photonics West BIOS*, S. (Ed.), San Francisco, USA, pp. 8226–8246.
- Latour, G., Gusachenko, I., Kowalczyk, L., Lamarre, I., Schanne-Klein, M.-C., 2012b. In vivo structural imaging of the cornea by polarization-resolved second harmonic microscopy. *Biomed. Opt. Express* 3, 1–15.
- Matteini, P., Ratto, F., Rossi, F., Cicchi, R., Stringari, C., Kapsokalyvas, D., Pavone, F.S., Pini, R., 2009. Photothermally-induced

- disordered patterns of corneal collagen revealed by SHG imaging. *Opt. Express* 17, 4868–4878.
- Meek, K.M., Boote, C., 2009. The use of X-ray scattering techniques to quantify the orientation and distribution of collagen in the corneal stroma. *Prog. Retin. Eye Res.* 28, 369–392.
- Meek, K.M., Tuft, S.J., Huang, Y.F., Gill, P.S., Hayes, S., Newton, R.H., Bron, A.J., 2005. Changes in collagen orientation and distribution in keratoconus corneas. *Investig. Ophthalmol. Vis. Sci.* 46, 1948–1956.
- Morishige, N., Shin-gyou-uchi, R., Azumi, H., Ohta, H., Morita, Y., Yamada, N., Kimura, K., Takahara, A., Sonoda, K.-H., 2014. Quantitative analysis of collagen lamellae in the normal and keratoconic human cornea by second harmonic generation imaging microscopy. *Investig. Ophthalmol. Vis. Sci.* 55, 8377–8385.
- Nahas, A., Bauer, M., Roux, S., Boccara, A.C., 2013. 3D static elastography at the micrometer scale using full field OCT. *Biomed. Opt. Express* 4, 2138–2149.
- Nguyen, T.-M., Aubry, J.-F., Fink, M., Bercoff, J., Tanter, M., 2014. In vivo evidence of porcine cornea anisotropy using supersonic shear wave imaging. *Investig. Ophthalmol. Vis. Sci.* 55, 7545–7552.
- Nguyen, T.D., Boyce, B.L., 2011. An inverse finite element method for determining the anisotropic properties of the cornea. *Biomech. Model. Mechanobiol.* 10, 323–337.
- Pandolfi, A., Vasta, M., 2012. Fiber distributed hyperelastic modeling of biological tissues. *Mech. Mater.* 44, 151–162.
- Petsche, S.J., Chernyak, D., Martiz, J., Levenston, M.E., Pinsky, P.M., 2012. Depth-dependent transverse shear properties of the human corneal stroma. *Investig. Ophthalmol. Vis. Sci.* 53, 873–880.
- Petsche, S.J., Pinsky, P.M., 2013. The role of 3-D collagen organization in stromal elasticity: a model based on X-ray diffraction data and second harmonic-generated images. *Biomech. Model. Mechanobiol.* 12, 1101–1113.
- Pinero, D.P., Alcon, N., 2014. In vivo characterization of corneal biomechanics. *J. Cataract Refract. Surg.* 40, 870–887.
- Pinsky, P.M., van der Heide, D., Chernyak, D., 2005. Computational modeling of mechanical anisotropy in the cornea and sclera. *J. Cataract Refract. Surg.* 31, 136–145.
- Plamann, K., Aptel, F., Arnold, C.L., Courjaud, A., Crotti, C., Deloison, F., Druon, F., Georges, P., Hanna, M., Legeais, J.M., Morin, F., Mottay, E., Nuzzo, V., Peyrot, D.A., Savoldelli, M., 2010. Ultrashort pulse laser surgery of the cornea and the sclera. *J. Opt.* 12, 30.
- Quantock, A.J., Winkler, M., Parfitt, G.J., Young, R.D., Brown, D.J., Boote, C., Jester, J.V., 2015. From nano to macro: studying the hierarchical structure of the corneal extracellular matrix. *Exp. Eye Res.* 133, 81–99.
- Radner, W., Zehetmayer, M., Aufreiter, R., Mallinger, R., 1998. Interlacing and cross-angle distribution of collagen lamellae in the human cornea. *Cornea* 17, 537–543.
- Roberts, C., 2000. The cornea is not a piece of plastic. *J. Refract. Surg.* 16, 7.
- Shin, T.J., Vito, R.P., Johnson, L.W., McCarey, B.E., 1997. The distribution of strain in the human cornea. *J. Biomech.* 30, 497–503.
- Stoller, P., Reiser, K.M., Celliers, P.M., Rubenchik, A.M., 2002. Polarization-modulated second harmonic generation in collagen. *Biophys. J.* 82, 3330–3342.
- Studer, H., Larrea, X., Riedwyl, H., Buechler, P., 2010. Biomechanical model of human cornea based on stromal microstructure. *J. Biomech.* 43, 836–842.
- Teulon, C., Gusachenko, I., Latour, G., Schanne-Klein, M.C., 2015. Theoretical, numerical and experimental study of geometrical parameters that affect anisotropy measurements in polarization-resolved SHG microscopy. *Opt. Express* 23, 9313–9328.
- Whitford, C., Studer, H., Boote, C., Meek, K.M., Elsheikh, A., 2015. Biomechanical model of the human cornea: considering shear stiffness and regional variation of collagen anisotropy and density. *J. Mech. Behav. Biomed. Mater.* 42, 76–87.
- Winkler, M., Shoa, G., Tran, S.T., Xie, Y., Thomasy, S., Raghunathan, V.K., Murphy, C., Brown, D.J., Jester, J.V., 2015. A comparative study of vertebrate corneal structure: the evolution of a refractive lens. *Investig. Ophthalmol. Vis. Sci.* 56, 2764–2772.
- Winkler, M., Shoa, G., Xie, Y., Petsche, S.J., Pinsky, P.M., Juhasz, T., Brown, D.J., Jester, J.V., 2013. Three-dimensional distribution of transverse collagen fibers in the anterior human corneal stroma. *Investig. Ophthalmol. Vis. Sci.* 54, 7293–7301.
- Yeh, A.T., Nassif, N., Zoumi, A., Tromberg, B.J., 2002. Selective corneal imaging using combined second-harmonic generation and two-photon excited fluorescence. *Opt. Lett.* 27, 2082–2084.